Supporting Information

Co single-atoms on ultrathin N-doped porous carbon via a biomass complexation strategy for high performance metal-air batteries

Yanqiu Wang,[a] Baoying Yu,[d] Kang Liu,[c] Xuetao Yang,[a] Min Liu,[c] Ting-Shan Chan,[e] Xiaoqing Qiu,[a] Jie Li,[a, *] and Wenzhang Li[a, b *]

[a] *School of Chemistry and Chemical Engineering, Central South University, Changsha, 410083, China*

[b] *Hunan Provincial Key Laboratory of Efficient and Clean Utilization of Manganese Resources, Central South University, Changsha, 410083, China*

[c] *School of Physics and Electronics, Central South University, Changsha, 410083, China*

[d] *Xiangya School of Medicine, Central South University, Changsha, 410083, China*

[e] *National Synchrotron Radiation Research Center, Taiwan, 101 Hsin Ann Road, Hsinchu Science Park, Hsinchu 300, Taiwan*

[*] *Corresponding author*.

E-mail addresses: lijieliu@csu.edu.cn (J. Li), liwenzhang@csu.edu.cn (W. Li).

Table of Contents

Physicochemical characterization

The morphology and construction of the as-prepared samples were studied by a scanning electron microscope (SEM, Nova Nano SEM 230), a transmission electron microscope (TEM), a high resolution transmission electron microscope (HRTEM, FEI TECNAI G2 F20) and Double Cs Corrector Transmission Electron Microscope (Themis Z). Atomic force microscopy (AFM, NanoMan VS) was implemented to ascertain the thickness messages of samples. The crystal structure of catalysts was analyzed by an X-ray diffractometer (SIMENS d500) and Raman spectra with a LabRAM Hr800 microscope at excitation laser of 532 nm. The actual Co content in the catalyst was measured by ICP-OES (inductively coupled plasma optical emission spectrometer, OPTIMA8000). The XPS (X-ray photoelectron spectroscopy) with the K-Alpha 1063 was applied to examine the surface composition and electronic structure of Co SANC. The specific surface area and pore size distribution of the samples were determined by N_2 sorption isotherms at 77 K (ASAP 2460 analyzer). The X-ray Absorption Fine Structure spectra of Co K-edge were recorded at the National Synchrotron Radiation Research Center (NSRRC) in Hsinchu. The Co K-edge XANES data were collected at a fluorescence mode using Co foil, CoO and Co_3O_4 as references. The collected EXAFS data were processed utilizing IFEFFIT program.

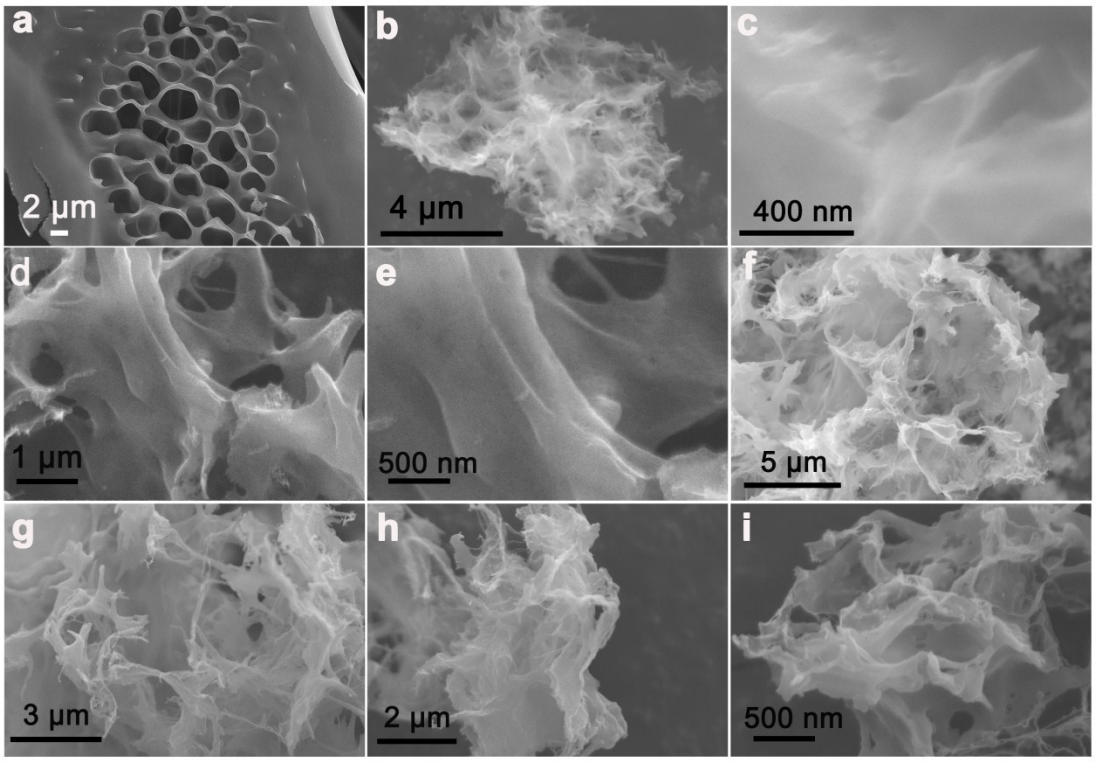

Fig. S1 (a) The SEM image of Co SANC-850-0 (without NH_4Cl under 850 °C), SEM images of (b, c) Co SANC-850, (d, e) Co SANC-750, (f, g) Co SANC-800 and (h, i) Co SANC-900

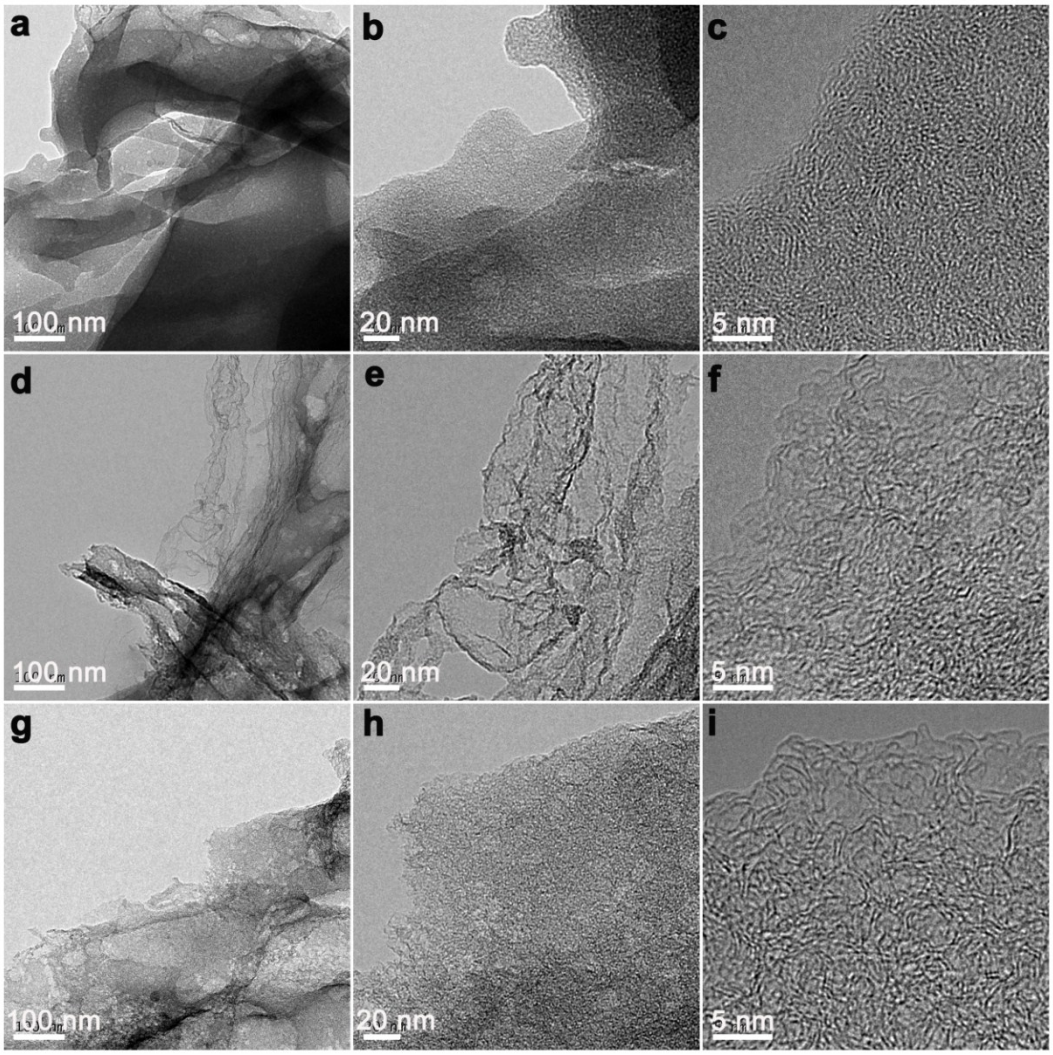

Fig. S2 TEM and HRTEM images of (a-c) Co SANC-750, (d-f) Co SANC-800 and (g-i) Co SANC-900

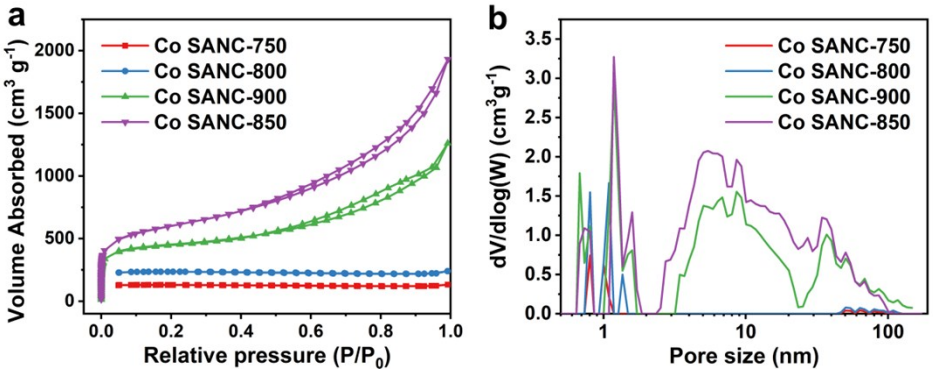

Fig. S3 (a) N_2 absorption/desorption isotherms and (b) pore size distribution plots for Co SANC-750, Co SANC-800, Co SANC-900 and CoSANC-850

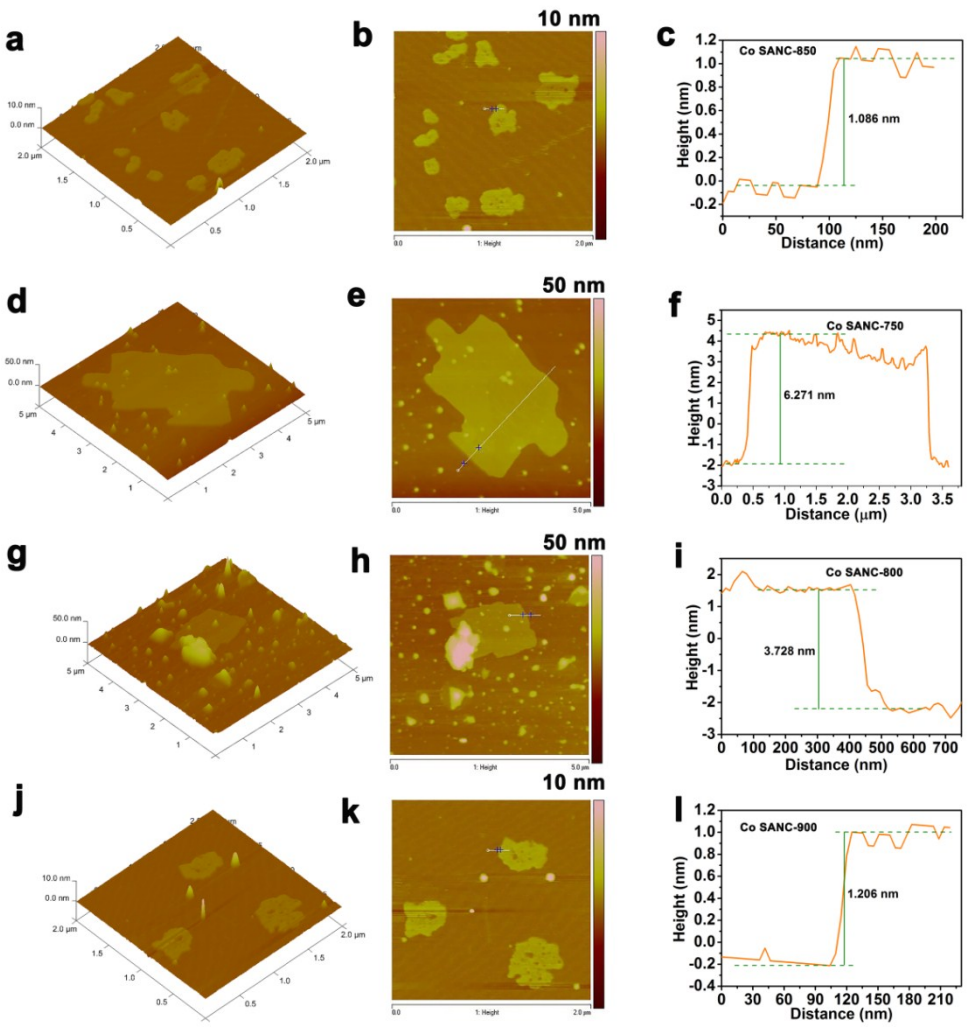

Fig. S4 AFM images of (a-c) Co SANC-850, (d-f) Co SANC-750, (g-i) Co SANC-800 and (j-l) Co SANC-900

Table S1 Cobalt contents of the various catalysts determined by XPS and ICP-OES

Sample	Co SANC-750	Co SANC-800	Co SANC-850	Co SANC-900
XPS (at%)	0.25	0.17	0.13	0.12
ICP-OES (wt%)	1.50	1.35	1.27	1.02

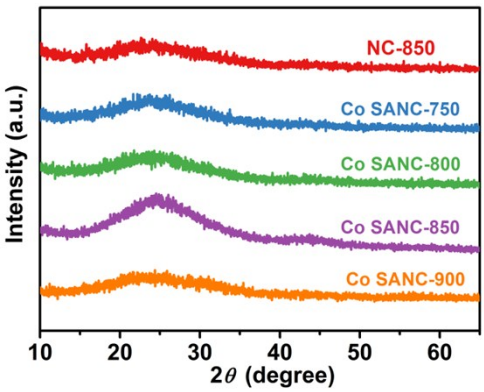

Fig. S5 XRD patterns of samples

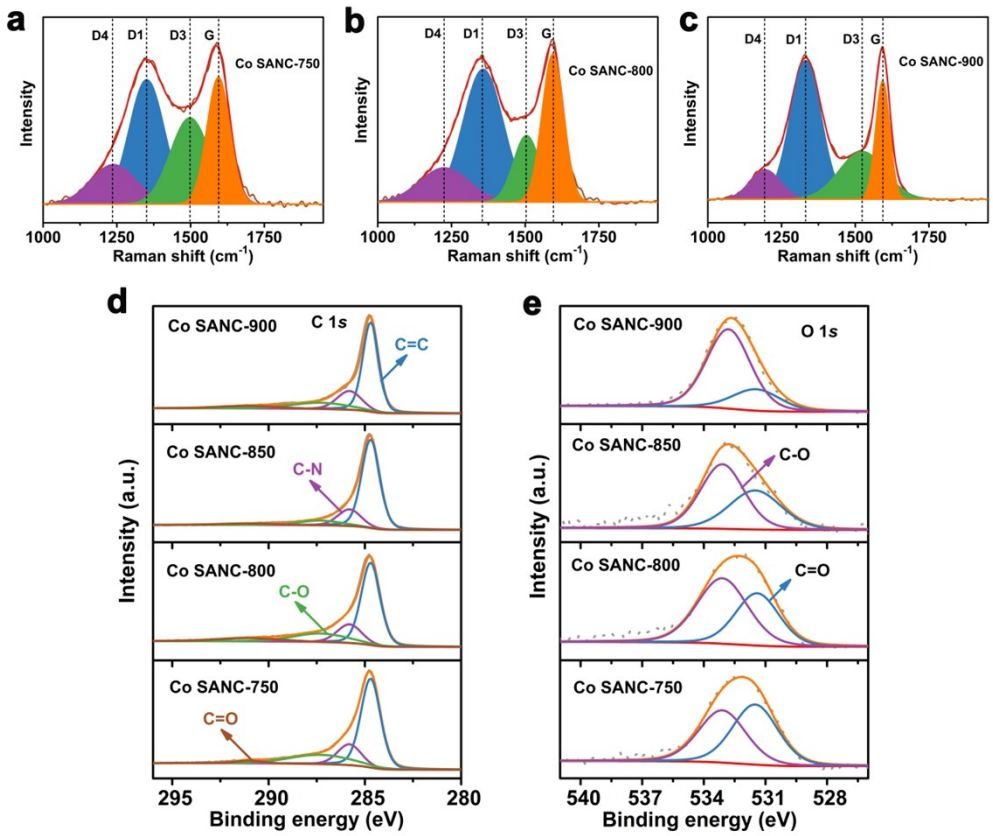

Fig. S6 (a-c) the fitting results of Raman spectra for Co SANC-750, Co SANC-800 and Co SANC-900, respectively, (d) C 1*s* and (e) O 1*s* high-resolution XPS spectra for Co SANC-750, Co SANC-800, Co SANC-850 and Co SANC-900

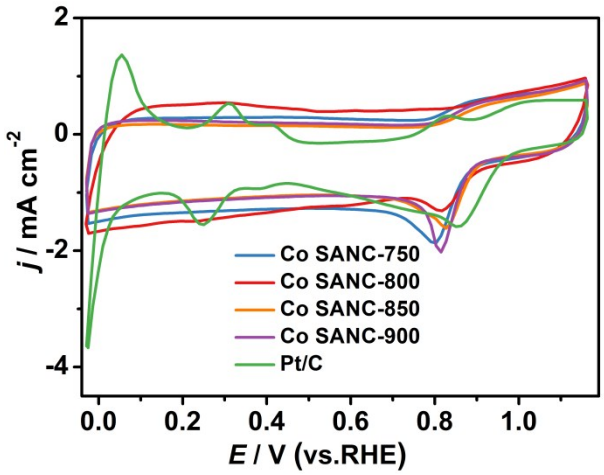

Fig. S7 (a) CV plots of samples in O_2-saturated 0.1 M KOH media

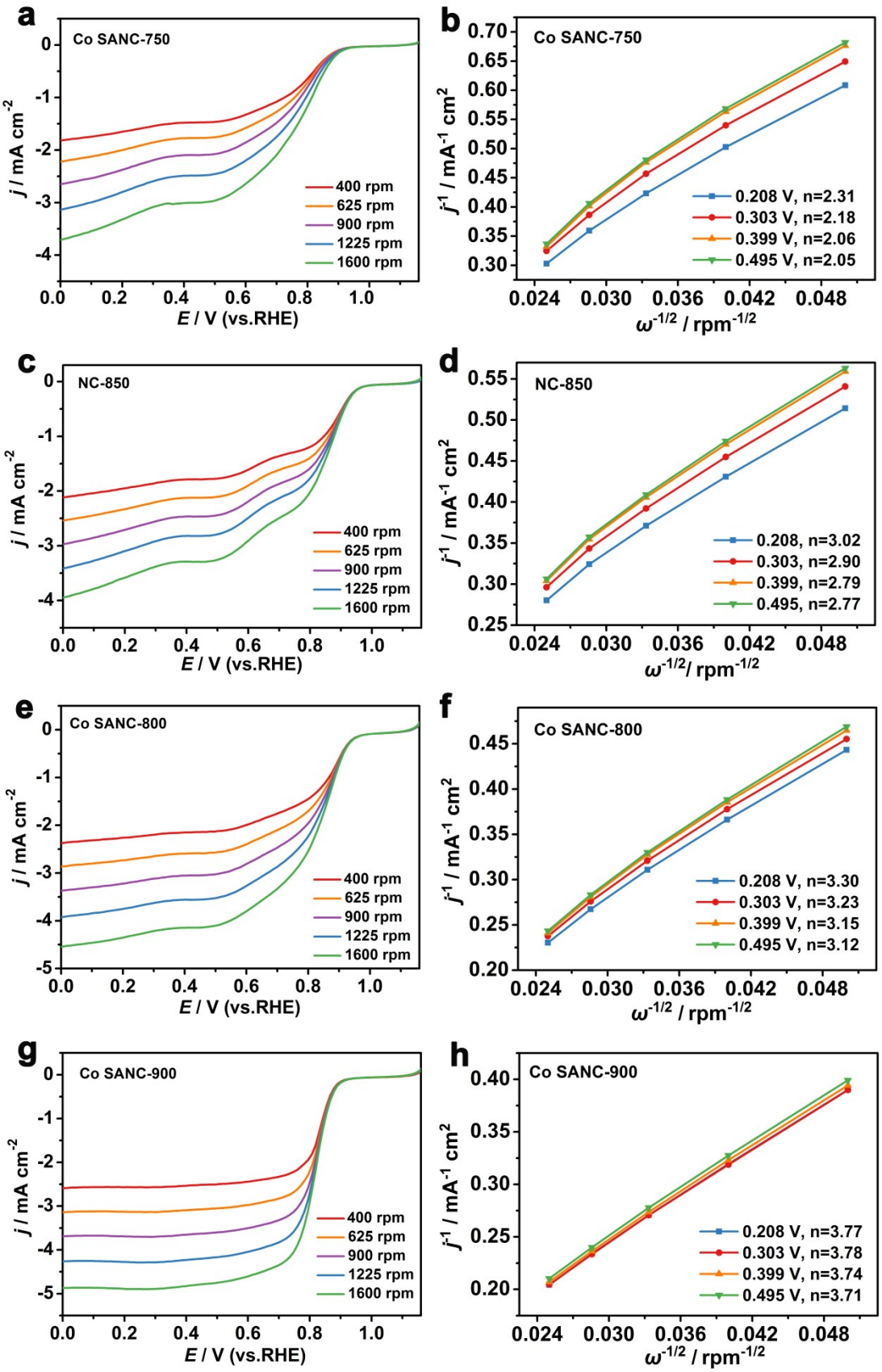

Fig. S8 (a, c, e and g) LSV curves at various rotation rates and (b, d, f and h) K-L plots at different potentials for Co-SANC-750, NC-850, Co-SANC-800 and Co-SANC-900 in O_2-saturated 0.1 M KOH solutions, respectively

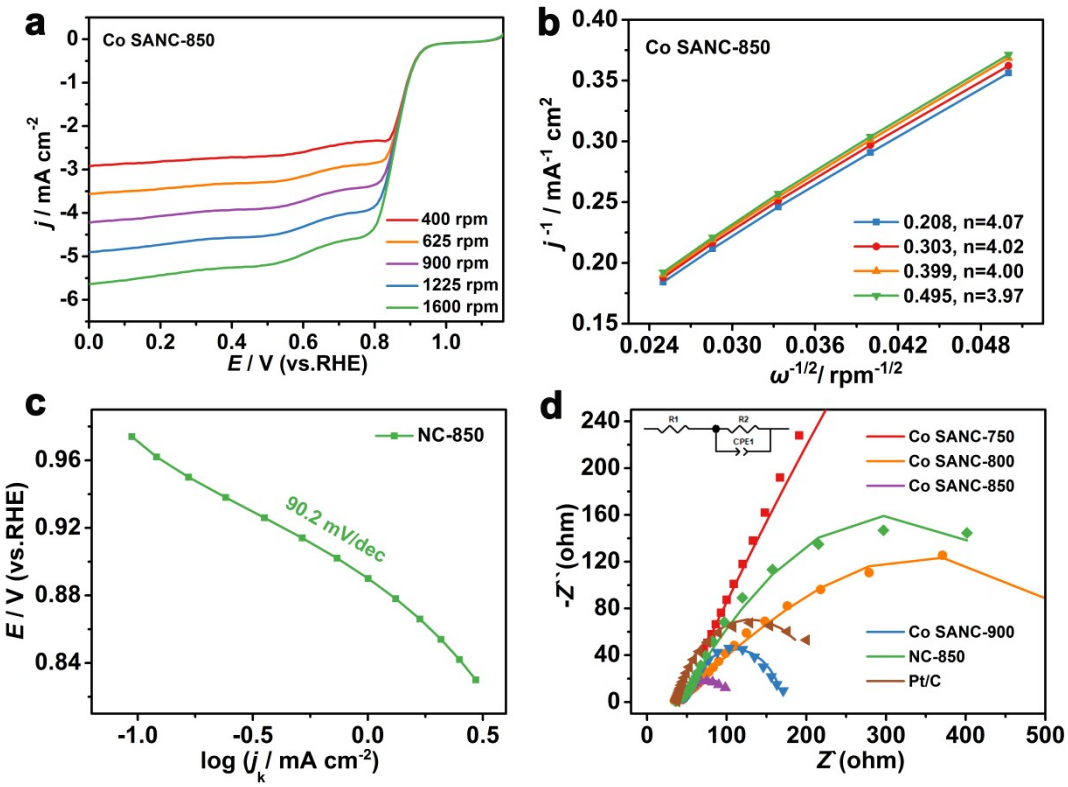

Fig. S9 (a, b) LSV and K-L plots for Co SANC-850, (c) Tafel plot of NC-850 and (d) Nyquist plots of samples (fitted curves, solid lines; experimental points, symbols). Inset is the equivalent circuit, where R1, R2 and CPE1 represent the inherent resistances of devices, charge-transfer resistance and double-layer capacitance resistance, respectively

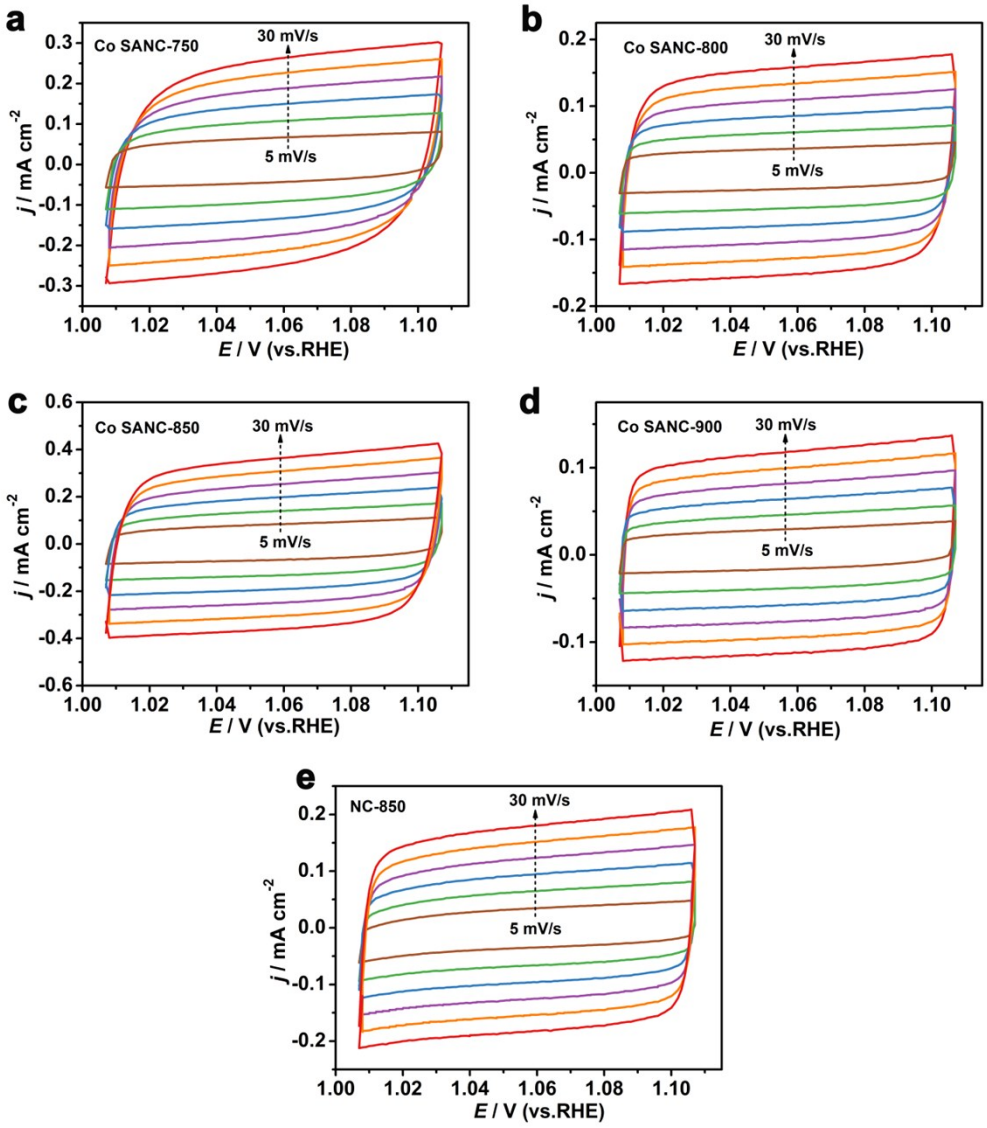

Fig. S10 CVs from 1.007 V to 1.107 V vs RHE under different scan rates (5, 10, 15, 20, 25 and 30 mV s^{-1}, respectively) for Co SANC-750, Co SANC-800, Co SANC-850, Co SANC-900 and NC-850.

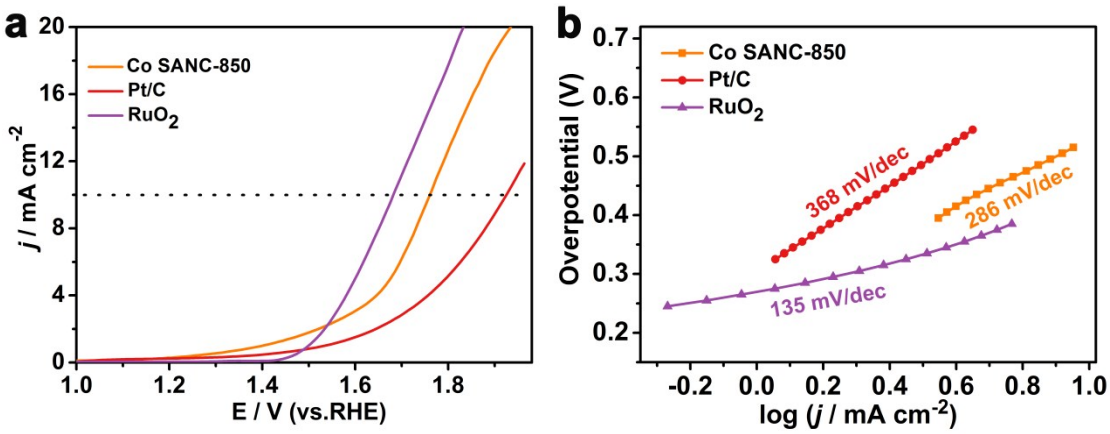

Fig. S11 (a) OER tests and (b) Tafel plots for Co SANC-850, Pt/C and RuO_2

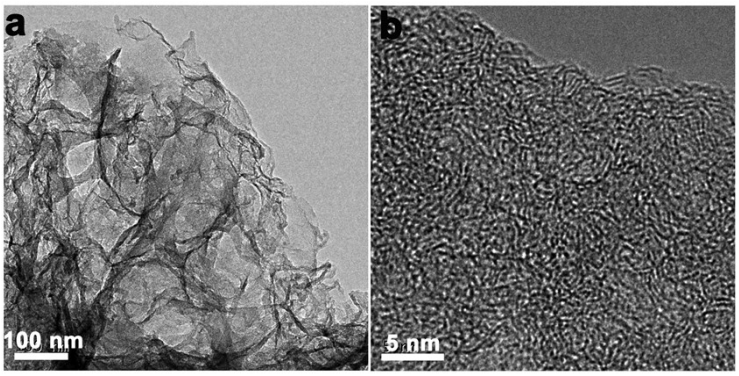

Fig. S12 (a, b) TEM and HRTEM images of Co SANC-850 after catalysis

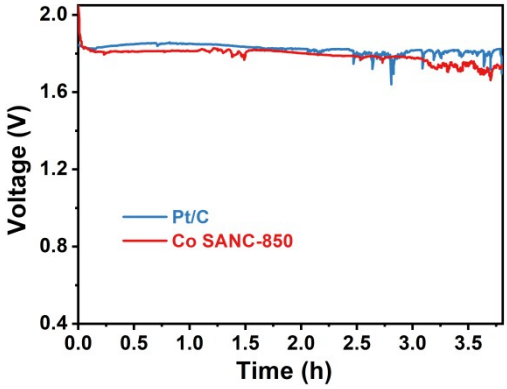

Fig. S13 Open-circuit voltage of Al-air battery

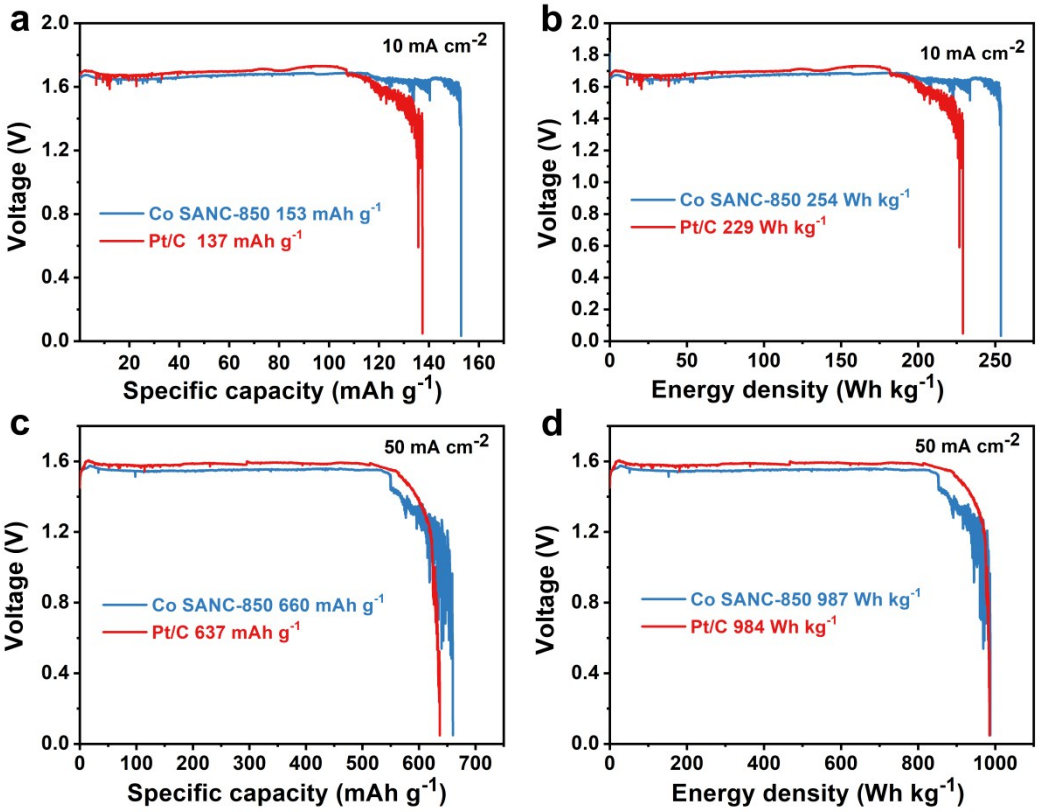

Fig. S14 (a, c) Specific capacities and (b, d) the corresponding energy densities for Co SANC-850 and Pt/C at 10 mA cm^{-2} and 50 mA cm^{-2} in Al-air battery, respectively

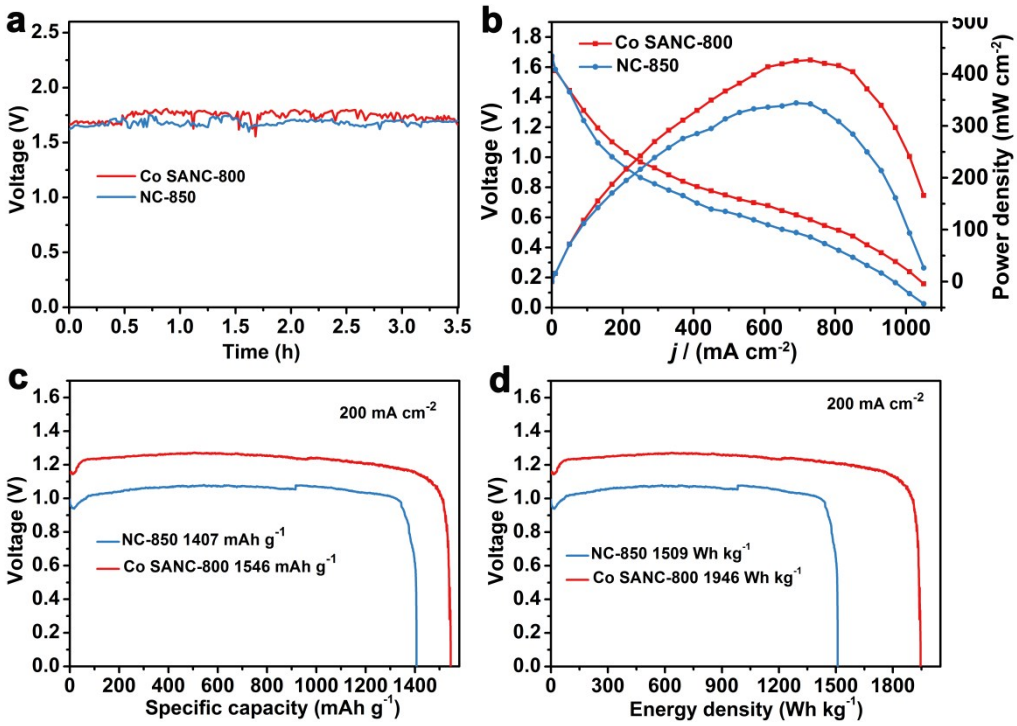

Fig. S15 Performance of Al-air battery (a) open-circuit voltage, (b) polarization and power density plots, (c) specific capacities and (d) corresponding energy density at 200 mA cm^{-2}, respectively.

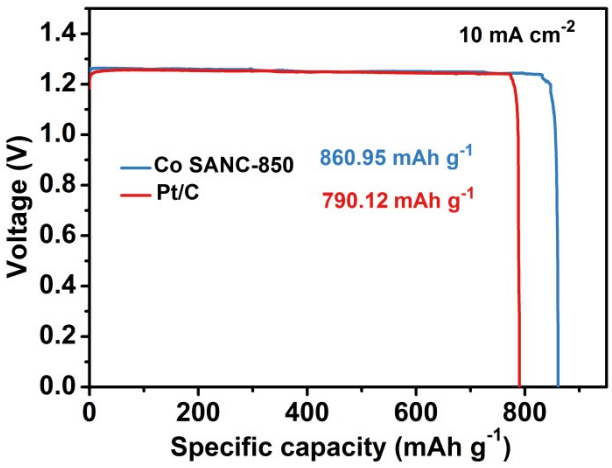

Fig. S16 Discharge curves of primary Zn-air battery for Co SANC-850 and Pt/C**.**

Theoretical Section

Density functional theory (DFT) calculations about the ORR mechanism were performed using the Vienna ab initio simulation package (VASP).[1] The projector-augmented wave (PAW) method was employed for describing the electron-ion interaction.[2] The generalized gradient approximation (GGA) of Perdew-Burke-

Ernzerhof (PBE) was used for estimating the electron-electron exchange and correlation functional.[3] In our calculation, we used plane-wave basis set with 400 eV kinetic energy cutoff and the Brillouin zone was sampled by the Monkhorst-Pack method with 3x3x1 k-point grids for Co-N_4, Graphitic N and Pyridinic N, respectively.

The Gibbs free energy change ΔG of each elementary step was calculated as:

$$\Delta G = \Delta E + \Delta ZPE - T \bullet \Delta S + \Delta G_U$$

Where T denotes the temperature of 298.15 K, ΔE is the reaction energy calculated by the DFT method, ΔZPE and ΔS are the changes in zero-point energies and entropy during the reaction, respectively.[4] $\Delta G_U = -neU$, it represents the applied potential (U) effect on reaction concerning electron (e) in the electrode and n is electron transfer number of elementary reaction.[5] The over-potential of the ORR can be determined by computing Gibbs free energies of the reaction at the different elementary steps. The thermochemistry of these reactions was obtained by DFT computations along with the computational hydrogen electrode (CHE) model exploited by Nørskov et al.[6] The electrochemical investigations have demonstrated that a $4e^-$ pathway proceeds for ORR and OER on the Co-N_4 based carbon catalyst. The thermodynamics of elementary reactions under acidic or alkaline environment is same.[7] Therefore, the $4e^-$ reaction mechanism about ORR in acidic condition could be as below:

$$O_2\,(g) + H^+ + e^- + {}^* \leftrightarrow {}^*OOH \qquad (S1)$$

$${}^*OOH + H^+ + e^- \leftrightarrow {}^*O + H_2O\,(l) \qquad (S2)$$

$$^{*}O + H^{+} + e^{-} \leftrightarrow {}^{*}OH \qquad (S3)$$

$$^{*}OH + H^{+} + e^{-} \leftrightarrow {}^{*} + H_2O\ (l) \qquad (S4)$$

Where * refers to active sites, (l) and (g) stand for liquid and gas phases, separately, $^{*}OOH$, $^{*}O$ and $^{*}OH$ represent adsorbed intermediates. As a reverse reaction of ORR, the mechanism of OER is describe as below:

$$H_2O\ (l) + {}^{*} \leftrightarrow {}^{*}OH + H^{+} + e^{-} \qquad (S5)$$

$$^{*}OH \leftrightarrow {}^{*}O + H^{+} + e^{-} \qquad (S6)$$

$$^{*}O + H_2O\ (l) \leftrightarrow {}^{*}OOH + H^{+} + e^{-} \qquad (S7)$$

$$^{*}OOH \leftrightarrow O_2\ (g) + H^{+} + e^{-} + {}^{*} \qquad (S8)$$

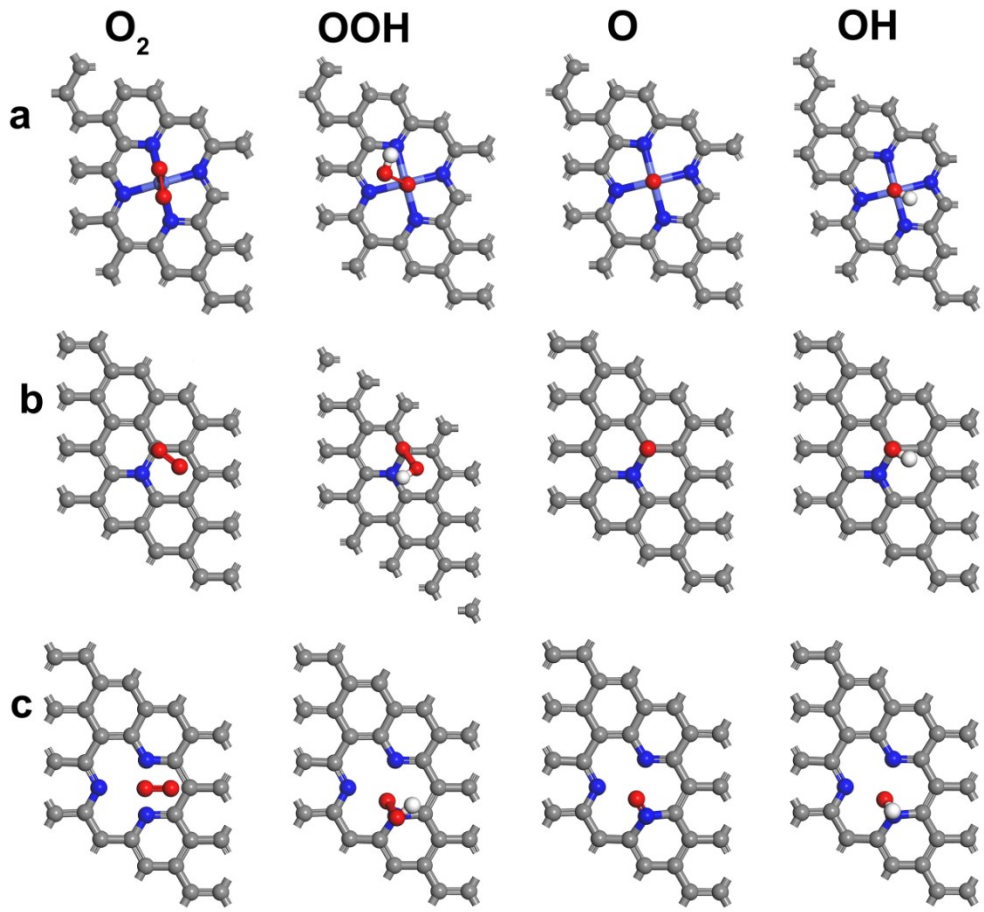

Fig. S17 Configurations of adsorbates on (a) Co-N_4, (b) graphitic N and (c) pyridinic N

Table S2 EXAFS data fitting outcomes of Co SANC-850

Sample	Path	Coordination number	R(Å)	DW factor (10^{-3} Å^2)	ΔE_0 (eV)	Residue
Co SANC-850	Co-N	4.16 ±0.275	1.878±0.007	0.093±0.012	-15.346	0.983

DW factor, Debye–Waller factor; R, the interatomic distance; ΔE_0, inner potential shift used in the fitting.

Table S3 Zero point energies (ZPE, eV), energy (E, eV) and entropy contribution (TS, eV) for OH, O and OOH intermediates on Co-N_4 structure site

Substrate	-278.974		
CoN_4	**E**	**ZPE**	**TS**
OOH	-293.506	0.4426	0.18917
O	-283.77	0.0595	0.071319
OH	-289.041	0.3345	0.162467

Table S4 Zero point energies (ZPE, eV), energy (E, eV) and entropy contribution (TS, eV) for OH, O and OOH intermediates on Graphitic N structure site

Substrate	-293.606		
Graphitic N	**E**	**ZPE**	**TS**
OOH	-307.545	0.4575	0.150118
O	-298.339	0.0709	0.021121
OH	-303.374	0.389	0.064948

Table S5 Zero point energies (ZPE, eV), energy (E, eV) and entropy contribution (TS, eV) for OH, O and OOH intermediates on Pyridinic N structure site

Substrate	-279.932		
Pyridinic N	**E**	**ZPE**	**TS**
OOH	-293.623	0.446	0.149128
O	-284.989	0.0937	0.041039
OH	-289.011	0.3977	0.062744

Table S6 Zero point energies (ZPE, eV), energy (E, eV) and entropy contribution (TS, eV) for H_2 and H_2O

	E	**ZPE**	**TS**
H_2	-6.75	0.27	0.41
H_2O	-14.21	0.56	0.67

Table S7 Reaction free energy (eV) of elementary step for 4 electron transfer ORR at U_{RHE}=0 V, pH=0 on various active sites

	Co-N_4	**Graphitic N**	**Pyridinic N**
Elementary reactions	**ΔG**	**ΔG**	**ΔG**
O_2 (g) + H^+ + e^- + * ↔ *OOH	-1.08	**-0.7**	-0.67
*OOH + H^+ + e^-↔ *O + H_2O (l)	-1.41	-1.92	-2.48
*O + H^+ + e^- ↔ *OH	-1.64	-1.32	**-0.3**
*OH + H^+ + e^-↔ * + H_2O (l)	**-0.98**	-1.43	-2.13

Table S8 Reaction free energy (eV) of elementary step for 4 electron transfer ORR at U_{RHE}=1.23 V, pH=0 on various active sites

	Co-N_4	**Graphitic N**	**Pyridinic N**
Elementary reactions	**ΔG**	**ΔG**	**ΔG**
O_2 (g) + H^+ + e^- + * ↔ *OOH	0.15	0.53	0.56
*OOH + H^+ + e^-↔ *O + H_2O (l)	-0.18	-0.69	-1.25
*O + H^+ + e^- ↔ *OH	-0.41	-0.09	0.93
*OH + H^+ + e^-↔ * + H_2O (l)	0.25	-0.2	-0.9

Table S9 Reaction free energy (eV) of elementary step for 4 electron transfer ORR at equilibrium potential, pH=0 on various active sites

	Co-N_4	**Graphitic N**	**Pyridinic N**
Elementary reactions	**ΔG**	**ΔG**	**ΔG**
O_2 (g) + H^+ + e^- + * ↔ *OOH	-0.1	0	-0.37
*OOH + H^+ + e^-↔ *O + H_2O (l)	-0.43	-1.22	-2.18
*O + H^+ + e^- ↔ *OH	-0.66	-0.62	0
*OH + H^+ + e^-↔ * + H_2O (l)	0	-0.73	-1.83

Table S10 Reaction free energy (eV) of elementary step for 4 electron transfer OER at U_{RHE}=0 V, pH=0 on various active sites

	Co-N_4	**Graphitic N**	**Pyridinic N**
Elementary reactions	**ΔG**	**ΔG**	**ΔG**
H_2O (l) + * ↔ *OH + H^+ + e^-	0.98	1.43	2.13
*OH ↔ *O + H^+ + e^-	**1.64**	1.32	0.3
*O + H_2O (l) ↔ *OOH + H^+ + e^-	1.41	**1.92**	**2.48**
*OOH ↔ O_2 (g) + H^+ + e^- + *	1.08	0.7	0.67

Table S11 Reaction free energy (eV) of elementary step for 4 electron transfer OER at U_{RHE}=1.23 V, pH=0 on various active sites

Elementary reactions	Co-N_4 ΔG	Graphitic N ΔG	Pyridinic N ΔG
H_2O (l) + * ↔ *OH + H^+ + e^-	-0.25	0.2	0.9
*OH ↔ *O + H^+ + e^-	0.41	0.09	-0.93
*O + H_2O (l) ↔ *OOH + H^+ + e^-	0.18	0.69	1.25
*OOH ↔ O_2 (g) + H^+ + e^- + *	-0.15	-0.53	-0.56

Table S12 Reaction free energy (eV) of elementary step for 4 electron transfer OER at equilibrium potential, pH=0 on various active sites

Elementary reactions	Co-N_4 ΔG	Graphitic N ΔG	Pyridinic N ΔG
H_2O (l) + * ↔ *OH + H^+ + e^-	-0.66	-0.49	-0.35
*OH ↔ *O + H^+ + e^-	0	-0.6	-2.18
*O + H_2O (l) ↔ *OOH + H^+ + e^-	-0.23	0	0
*OOH ↔ O_2 (g) + H^+ + e^- + *	-0.56	-1.22	-1.81

Table S13 Comparative summary of the performance for primary Al-air batteries with the present work

Catalyst	Electrolyte	Discharge voltage (V)	Current densities (mA cm^{-2})	Peak power density (mW cm^{-2})	Energy density (Wh kg^{-1})	Ref.
Co SANC-850	6 M KOH + 0.01 M Na_2SnO_3 + 0.0005 M $In(OH)_3$+ 0.0075 M ZnO	**1.33**	**200**	**494**	**2387**	**This work**
Co_3O_4/N-KB	6 M KOH + 0.01 M Na_2SnO_3 + 0.0005 M $In(OH)_3$+ 0.0075 M ZnO	1.50	50	161.1	\	8
Cu-Fe-N-C	6 M KOH + 0.01 M Na_2SnO_3 + 0.0005 M $In(OH)_3$ + 0.0075 M ZnO	1.64	20	\		9
CuNC/KB	6 M KOH + 0.01 M Na_2SnO_3 + 0.0005 M $In(OH)_3$ + 0.0075 M ZnO	1.53	40	\	\	10
Ag/Fe_3O_4/N-KB	6 M KOH + 0.01 M Na_2SnO_3 + 0.0005 M $In(OH)_3$ + 0.0075 M ZnO	1.49	50	\	\	11
$NiCo_2O_4$/CNTs	6 M KOH + 0.01 M Na_2SnO_3 + 0.0005 M $In(OH)_3$ + 0.0075 M	1.20	200	\	\	12

Ag/CNT sheets	ZnO PVA + PEO + KOH + ZnO + Na_2SnO_3 (hydrogel)	1.29	0.5	1.33	1168	[13]
Ag/MnO_2	4 M KOH	1.31	100	204	\	[14]
Co_3O_4-CeO_2/KB	6 M KOH + 0.01 M Na_2SnO_3 + 0.0005 M $In(OH)_3$ + 0.0075 M ZnO	1.27	50	\	\	[15]
Co_3O_4/N-KB	6 M KOH + 0.01 M Na_2SnO_3 + 0.0005 M $In(OH)_3$ + 0.0075 M ZnO	1.52	20	\	\	[16]
Cu-N-KB	6 M KOH + 0.01 M Na_2SnO_3 + 0.0005 M $In(OH)_3$ + 0.0075 M ZnO	1.47	50	\	\	[17]
Ag-CeO_2/VXC-72	4 M KOH	1.50	100	345	\	[18]

Table S14 Comparative summary of the performance for rechargeable Zn-air batteries with the present work

Catalyst	Open circuit voltage (V)	Discharge voltage (V)	Current density (mA cm^{-2})	Initial round-trip efficiency	Cycling current density (mA cm^{-2})	Ref.
Co SANC-850	**1.48**	**1.21**	**10**	**60.8 %**	**10**	**This work**
Pt/C+RuO_2	1.45	1.21	10	60.5 %	10	This work
Co-N,B-CSs	1.43	1.20	10	58 %	5	[19]
FeNC-S-Fe_xC/Fe	1.41	1.21	10	55.6 %	2	[20]
NiO/CoN PINWs	1.46	0.19	10	37.5 %	3	[21]
A-Co@CMK-3-D	\	1.1	10	50 %	10	[22]
NGM-Co	\	1.12	20	48.9 %	5	[23]
CoO/N-CNT+FeNi LDH/CNT	\	1.2	50	65 %	20	[24]
$Co(OH)_2$/CoPt/N-CN	\	\	\	60 %	10	[25]
Co-N_x/C NRA	1.42	\	\	64.8 %	5	[26]
1 nm-CoO_x/N-RGO	1.39	\	\	68.7 %	6	[27]
NCN-1000-80	1.44	1.21	10	61.1 %	10	[28]
Co SA@NCF/CNF	1.41	\	\	67.6 %	6.25	[29]

Supplementary References

1. G. Kresse and J. Hafner, *Phys. Rev. B*, 1994, **49**, 14251-14269.
2. P. E. Blöchl, *Phy. Rev. B*, 1994, **50**, 17953-17979.
3. J. P. Perdew, K. Burke and M. Ernzerhof, *Phys. Rev. lett.*, 1996, **77**, 3865.
4. J. K. Nørskov, T. Bligaard, A. Logadottir, J. Kitchin, J. G. Chen, S. Pandelov and U. Stimming, *J. Electrochem. Soc.*, 2005, **152**, J23-J26.
5. L. Yang, D. Cheng, H. Xu, X. Zeng, X. Wan, J. Shui, Z. Xiang and D. Cao, *Proc. Natl. Acad. Sci.*, 2018, **115**, 6626-6631.
6. J. K. Nørskov, J. Rossmeisl, A. Logadottir, L. Lindqvist, J. R. Kitchin, T. Bligaard and H. Jonsson, *J. Phys. Chem. B*, 2004, **108**, 17886-17892.
7. Y. Chen, S. Ji, Y. Wang, J. Dong, W. Chen, Z. Li, R. Shen, L. Zheng, Z. Zhuang, D. Wang and Y. Li, *Angew. Chem., Int. Ed.* , 2017, **56**, 6937-6941.
8. J. Li, Z. Zhou, K. Liu, F. Li, Z. Peng, Y. Tang and H. Wang, *J. Power Sources*, 2017, **343**, 30-38.
9. J. Li, J. Chen, H. Wan, J. Xiao, Y. Tang, M. Liu and H. Wang, *Appl. Catal., B*, 2019, **242**, 209-217.
10. J. Li, N. Zhou, J. Song, L. Fu, J. Yan, Y. Tang and H. Wang, *ACS Sustain. Chem. Eng.*, 2017, **6**, 413-421.
11. F. Li, L. Fu, J. Li, J. Yan, Y. Tang, Y. Pan and H. Wang, *J. Electrochem. Soc.*, 2017, **164**, A3595-A3601.
12. H. Zhang, H. Qiao, H. Wang, N. Zhou, J. Chen, Y. Tang, J. Li and C. Huang, *Nanoscale*, 2014, **6**, 10235-10242.
13. Y. Xu, Y. Zhao, J. Ren, Y. Zhang and H. Peng, *Angew. Chem. Int. Ed.* , 2016, **55**, 7979-7982.
14. S. Sun, H. Miao, Y. Xue, Q. Wang, S. Li and Z. Liu, *Electrochim. Acta*, 2016, **214**, 49-55.
15. K. Liu, X. Huang, H. Wang, F. Li, Y. Tang, J. Li and M. Shao, *ACS Appl. Mater. Interfaces*, 2016, **8**, 34422-34430.
16. K. Liu, Z. Zhou, H. Wang, X. Huang, J. Xu, Y. Tang, J. Li, H. Chu and J. Chen, *Rsc Advances*, 2016, **6**, 55552-55559.
17. F. Li, J. Li, Q. Feng, J. Yan, Y. Tang and H. Wang, *J. Energy Chem.*, 2018, **27**, 419-425.
18. S. Sun, Y. Xue, Q. Wang, S. Li, H. Huang, H. Miao and Z. Liu, *Chem Commun*, 2017, **53**, 7921-7924.
19. Y. Guo, P. Yuan, J. Zhang, Y. Hu, I. S. Amiinu, X. Wang, J. Zhou, H. Xia, Z. Song, Q. Xu and S. Mu, *ACS Nano*, 2018, **12**, 1894-1901.
20. Y. Qiao, P. Yuan, Y. Hu, J. Zhang, S. Mu, J. Zhou, H. Li, H. Xia, J. He and Q. Xu, *Adv. Mater.*, 2018, **30**, 1804504.
21. J. Yin, Y. Li, F. Lv, Q. Fan, Y. Q. Zhao, Q. Zhang, W. Wang, F. Cheng, P. Xi and S. Guo, *ACS Nano*, 2017, **11**, 2275-2283.
22. X. Lyu, G. Li, X. Chen, B. Shi, J. Liu, L. Zhuang and Y. Jia, *Small Methods*, 2019, 1800450.

23. C. Tang, B. Wang, H. F. Wang and Q. Zhang, *Adv. Mater.*, 2017, **29**, 1703185.
24. Y. Li, M. Gong, Y. Liang, J. Feng, J.-E. Kim, H. Wang, G. Hong, B. Zhang and H. Dai, *Nat. Commun.*, 2013, **4**, 1805.
25. K. Wang, W. Wu, Z. Tang, L. Li, S. Chen and N. M. Bedford, *ACS Appl. Mater. Interfaces*, 2019, **11**, 4983-4994.
26. I. S. Amiinu, X. Liu, Z. Pu, W. Li, Q. Li, J. Zhang, H. Tang, H. Zhang and S. Mu, *Adv. Funct. Mater.*, 2018, **28**, 1704638.
27. T. Zhou, W. Xu, N. Zhang, Z. Du, C. Zhong, W. Yan, H. Ju, W. Chu, H. Jiang, C. Wu and Y. Xie, *Adv. Mater.*, 2019, **31**, e1807468.
28. H. Jiang, J. Gu, X. Zheng, M. Liu, X. Qiu, L. Wang, W. Li, Z. Chen, X. Ji and J. Li, *Energy Environ. Sci.*, 2019, **12**, 322-333.
29. D. Ji, L. Fan, L. Li, S. Peng, D. Yu, J. Song, S. Ramakrishna and S. Guo, *Adv. Mater.*, 2019, **31**, 1808267.